From polysaccharides to UV-curable biorenewable organo/hydrogels for methylene blue removal

# From polysaccharides to UV-curable biorenewable organo/hydrogels for methylene blue removal

*Camilla Noè*[a], *Andrea Cosola*[a], *Annalisa Chiappone*[a,b], *Minna Hakkarainen*[c], *Hansjörg Grützmacher*[d], *Marco Sangermano**[a]

[a]Department of Applied Science and Technology, Politecnico di Torino, C.so Duca degli Abruzzi 24, 10129 Torino, Italy

[b]POLITO BIOMedLAB, Politecnico di Torino, Turin, Italy

[c]KTH Royal Institute of Technology, Department of Fibre and Polymer Technology, Teknikringen 56-58, 10044 Stockholm, Sweden

[d]Department of Chemistry and Applied Biosciences, ETH Zurich, 8093 Zurich, Switzerland

KEYWORDS: UV-curing, polysaccaharides, hydrogels

ABSTRACT

Biorenewable "all-starch"-derived organo/hydrogels (OHGs) were prepared *via* "green" and fast UV-curing and tested as bio-adsorbents for the removal of methylene blue from water. Methacrylated starch (MS) and acrylated starch derivative, γ-cyclodextrin (ACy), were synthetized

for use as ~~hydrogel~~ OHG precursors for the photopolymerization process. Real-time photorheology confirmed the high reactivity of the prepared photocurable precursors. The mechanical properties and swelling behaviour of the photocured ~~hydrogels~~OHGs were examined focusing on the influence of the increasing amount of ACy. The MS-ACy ~~hydrogels~~OHGs were tested as innovative and environmental-friendly biorenewable materials for water treatment, using methylene blue (MB) as reference pollutant. The experimental data reveal that ~~hydrogels~~ OHGs containing an increasing amount of ACy show not only superior mechanical strength but also adsorption properties as a consequence of the high crosslinking efficiency of the acrylated cyclodextrin derivative and its ability to form host-guest inclusion complexes. Finally, the printability of these photocurable formulations *via* digital light processing (DLP) 3D – Printing is confirmed, envisaging ~~which allows to foresee~~ the fabrication of ~~new absorption~~absorbing materials with complex ~~but designed geometries for a specific application~~and application-tailored geometry, which could represent a new frontier ~~and as such offers new perspectives~~ for wastewater treatment.

## 1. INTRODUCTION

Water is the most valuable resource for mankind and water pollution caused by human activities is without question a major environmental problem. Among all aquatic pollutants, dyes take an ever-growing part and currently their world-wide annual production has reached approximately 800,000 tons whereby about 10-15% is lost into the environment during their industrial production [1]. Many dyes are commonly used in various large-scale industrial commodities such as in textiles, leather, food, paper printing, pharmaceuticals and cosmetics

[2,3]. Specifically, textile industry remains the major source of dye-release into the environment due to the considerable amount of water involved in the dyeing process [4]. As an example, 100 L of water is required to process 1 kg of textiles in traditional textile finishing processes [5]. The presence of coloured effluents inhibits the growth of the aquatic flora since they limit the sunlight penetration into waters, thus hindering photosynthesis and reducing the gas solubility in water [6]. Moreover, most synthetic dyes can cause hazards to humans due to their intrinsic toxicity. Among commercial dyes, 3,7-bis(dimethylamino) phenazathionium chloride, commonly known as methylene blue (MB), is one of the most used ones. Since it may provoke vomit, gastritis, cyanosis, heartbeat increase, jaundice, and tissue necrosis [7,8], its discharge even in traces into wastewater needs to be minimized.

Different processes are currently available for the removal of dye residues from water, such as chemical oxidation, adsorption, precipitation, membrane-filtration, electrolysis, photodegradation, electrokinetic coagulation, flocculation with Fe(II)/$Ca(OH)_2$, and also biological, microbiological, and physiochemical methods [9]. Despite that, many of the existing approaches have limitations associated to both the production of hazardous by-products and high energy costs. Among them, adsorption processes are extensively used since they are simple and cost-effective. Evidently, the adsorption efficiency largely relies on the type of adsorbent. Activated carbon, mesoporous silica, and magnetic nanoparticles are the most commonly used materials due to their high adsorption capacity and availability [10-12]. With the aim to develop low-cost adsorbent materials, several studies have been carried out to evaluate the adsorption properties of new polymeric hydrogels [13].

Hydrogels (HS) are three-dimensional hydrophilic crosslinked polymer networks able to absorb large quantities of water without dissolving. Therefore, they are gaining increasing

attention as adsorbents also for wastewater treatment. However, HS are commonly made of petroleum-based and non-degradable polymers, generating so-called secondary environmental pollution [14,15]. This is the reason why in the last years special attention has been given to adsorbents which are based naturally occurring resources, e.g. carbohydrate-based HS. These are environmentally friendly, renewable, biodegradable and non-toxic [16,17]. Several polysaccharides like cellulose [18], chitosan [19,20], starch [21], alginate [22], and dextran [23] were recently proposed for preparation of low-cost hydrogels [16,24]. Presently, these types of materials display low mechanical properties which hinder their applicability. Different strategies can be applied to overcome this problem, like the creation of double-crosslinked networks or the formation of hybrid hydrogels based on the combination of inorganic and organic materials [24,25].

Starch, in particular, is one of the most abundantly available polysaccharides. It consists of a mixture of two glucose-derived polymers, namely amylose (linear) and amylopectin (branched), joined together by α(1–4) linkages. Moreover, the high availability of hydroxyl groups makes it a very versatile biopolymer, giving the opportunity of chemical modifications *via* -OH substitution to prepare a large number of derivatives. And indeed, grafted starch has been previously used for the removal of metal [26,27] and dye pollutants from water [25].

Among starch derivatives, cyclodextrins (CDs), have been proposed as especially interesting absorbents. CDs are cyclic oligoamyloses, which can be sustainably derived from starch using glycosyltransferase and consist of either 6 (α), 7 (β) or 8 (γ) glucose subunits [28,29]. Taking advantage of their torus-shaped structure, they can be used to trap different pollutants *via* the generation of the so-called host-guest inclusion complexes [30,31]. Generally, different crosslinkers and grafting agents are used along with CDs to prepare grafted polymers or

copolymers. One of the first CD-based polymers being used for water purification consisted of CDs crosslinked with epichlorohydrin (ECH) [31-33]. Subsequently, various types of molecular architectures were developed by simply substituting the hydroxyl moieties of CDs with other functional groups, to make them suitable for different types of reaction with other polymers [33-37]. In particular, bio-based hydrogels prepared by using the CDs along with other natural polymers have shown promising potential in wastewater treatment [38,39]. However, the vast majority of investigations on hydrogels containing CDs focused on chitosan-based systems [40-43], while investigations combining CDs with other polysaccharides such as cellulose, starch, alginate and cotton are still scarce [37,44].

So far only few reports mentioned the use of bio-based photo-crosslinked hydrogels for wastewater treatment [45-47] and only one utilized photo-crosslinked polysaccharides [48]. Photopolymerizations have several advantages over other conventional techniques used to prepare chemically crosslinked hydrogels, namely fast reaction rates, no volatile organic compound (VOC) emissions, and no need of heat but comparatively low energy consumption [49-51].

We therefore synthesized new UV-curable polysaccharide-based organo/hydrogels (OHGs) from starch and γ-cyclodextrin. For this purpose, starch was methacrylated (methacrylated starch, MS) and γ-cyclodextrin acrylated (acrylated γ-cyclodextrin, ACy) according to previously reported procedures [51,52]. This procedure makes these molecules suitable for photopolymerization processes. The aim was to obtain a randomly oriented double network upon UV-light irradiation of the functionalized polysaccharides. Besides the function as absorbents, ACys could potentially reinforce the ~~hydrogel~~ OHG networks, due to the expected and already proven high crosslinking efficiency [52].

The curing kinetics of the photocurable formulations were evaluated *via* real-time photo-rheology. The mechanical properties and the swelling capability of the photocured ~~hydrogels~~ OHGs were investigated with the particular aim to characterize the structure of the crosslinked networks. Finally, the adsorption properties were investigated in detail to prove the potential application as bio-based absorbent material for waste-water treatment. Methylene blue (MB) was used as a model molecule for cationic dyes. Both the capacity and the kinetics of absorption of the MS-ACy ~~hydrogels~~ OHGs were investigated. Finally, the printability *via* digital light processing (DLP) 3D – Printing was demonstrated, envisaging a new frontier for wastewater treatment through fabrication of complex application-tailored geometries with increased surface area which may have a profound positive impact on the development of better performing absorption materials in general [53].

## 2. EXPERIMENTAL SECTION

### 2.1 Materials.

High amylose Hylon VII maize starch (70% amylose) was obtained from Ingredion (Goole, UK). γ-Cyclodextrin was obtained from ABCR. Methacrylic anhydride (MA), triethylamine (>99%) (TEA), dimethyl sulfoxide (DMSO) (ACS reagent P99.9%), ethanol absolute, acryloyl chloride, anhydrous n-methyl-pyrrolidone (NMP), methylene blue (MB), methyl red and phenylbis(2,4,6-trimethylbenzoyl)phosphine oxide (BAPO) were purchased from Sigma Aldrich and used without further purification.

### 2.2 Synthesis of methacrylate starch (MS)

Methacrylated starch (MS) was synthetized as previously reported [51]. Accordingly, 6 g of high amylose maize starch were dispersed in 200 mL of DMSO. Subsequently the solution was heated up at 70°C for 30 min to gelatinize the starch. Then, the solution was cooled down at room temperature (RT) and 12 mL of MA and 0.22 mL of TEA were added dropwise. The reaction was left to stir at RT for 18 hours. The products were then precipitated in ethanol, dissolved in deionized water and precipitate again in ethanol. This procedure was repeated two times in order to purify the product (47%). The final aqueous solution was lyophilized.

### 2.3 Synthesis of acrylated γ-cyclodextrin (ACy)

Acrylated γ-cyclodextrin (ACy) was prepared as previously reported [52]. Accordingly, γ-cyclodextrin (20 g) was first dried under high vacuum before being dissolved in anhydrous n-methyl-pyrrolidone (NMP, 160 mL). Then, the temperature was decreased to 0 °C and acryloyl chloride (36.07 mL) was added dropwise. The reaction mixture was magnetically stirred at RT for 72 h at 300 rpm. Dropping the reaction mixture into 2 L of deionized $H_2O$ gave ACy as a precipitate (67%). After decanting at RT for 30 min., the product was filtered and washed four times using deionized $H_2O$, before being dried under high vacuum for 24 h.

### 2.4 Organo/hydrogel preparation

Different photocurable formulations were prepared by dissolving the functionalized polysaccharide precursors in a $H_2O$/DMSO (20/80) mixture. The MS-ACy weight ratio was varied, while the total monomer concentration was kept at 10 wt% (Table 1). BAPO [1 phr, (weight per hundred resin)] was used as a photoinitiator. The ~~hydrogels~~ OHGs were prepared by pouring the precursor formulations into a silicon mold and irradiating for 1 minute with UV light

(100 mW/cm$^2$) using a Hamamatsu LC8 lamp equipped with 8 mm light guide (240 to 400 nm as spectral distribution).

**Table 1.** Photocurable formulations.

| Sample name | Methacrylated Starch (MS) (wt%) | Acrylated γ-Cyclodextrin (ACy) (wt%) | BAPO (phr) |
|---|---|---|---|
| **MS** | 100 | 0 | 1 |
| **MS-ACy 3-1** | 75 | 25 | |
| **MS-ACy 2-1** | 66 | 34 | |
| **MS-ACy 1-1** | 50 | 50 | |
| **MS-ACy 1-2** | 34 | 66 | |
| **ACy** | 0 | 100 | |

## 2.5 Characterization

### 2.5.1 Nuclear Magnetic Resonance (NMR)

$^1$H-NMR and $^{13}$C-NMR spectra were recorded on a Bruker Advance 400 Fourier Transform NMR spectrometer (FT NMR, Bruker, Billerica, MA, USA). The chemical shifts (δ) were measured and are given in parts per million (ppm) relative to TMS for $^1$H NMR and $^{13}$C{$^1$H} NMR, respectively, according to IUPAC. All the spectra were recorded at RT except for the $^{13}$C-NMR spectra of starch and methacrylated starch which were measured at 60°C to improve the spectra resolution.

### 2.5.2 Attenuated Total Reflectance-Fourier Transform Infrared Spectroscopy (ATR-FTIR)

FTIR spectra were recorded by using a Perkin Elmer Spectrum 2000 FTIR spectrometer (Perkin Elmer, Norwalk, CT, USA) equipped with a single reflection attenuated total reflectance (ATR) accessory (golden gate). 32 scans were recorded for each sample from 4000 to 500 cm$^{-1}$ with a resolution of 4 cm$^{-1}$.

### 2.5.3 Photorheology and Rheology

The rheology tests were performed using Anton PAAR Modular Compact Rheometer (Physica MCR 302, Graz, Austria) in a parallel plate configuration with a quartz bottom glass (25 mm). The experiments were recorded at RT setting the gap between the plates at 300 µm. Preliminary amplitude sweep measurements were conducted to define the linear viscoelastic region (LVR) of the liquid formulations. Real-time photorheology measurements were carried out to evaluate the curing kinetic of the precursor formulations. The curing process was evaluated by following the changes in the elastic storage modulus G' during UV-light irradiation (Hamamatsu LC8 lamp, 30 mW/cm$^2$). The tests were performed in the LVR setting a constant strain amplitude of 0.5% and constant frequency (ω) of 6 rad/s. The light was switched on after 30 s to let the system stabilize before the onset of polymerization. Frequency sweep experiments [ω: 0.1–100 rad/s] were then conducted on freshly crosslinked hydrogels under constant strain amplitude (1%). Finally, the main structural parameters of the crosslinked hydrogels were calculated as follows. The molar mass between two entanglement points ($M_e$*), the ~~crosslinking density~~numbers of crosslinks ($v_e$) and distance between two entanglement points (ξ) were obtained from equations 1, 2, and 3, respectively.

$$M_e^* = \frac{cRT}{G_p'} \quad (1)$$

$$v_e = \frac{G_p' N_A}{RT} \quad (2)$$

$$\xi = \frac{1}{\sqrt[3]{v_e}} \quad (3)$$

Where c is the concentration, R is the universal gas constant, T is the temperature in Kelvin, $G'_p$ is the storage modulus in the frequency independent plateau region and $N_A$ is the Avogadro's number [54].

### 2.5.4 Compression Test

Unconfined uniaxial compression tests were performed with a MTS QTestTM/10 Elite controller using TestWorks® 4 software (MTS Systems Corporation, Edan Prairie, Minnesota, USA). The measurements were performed at RT on cylindrical samples (⌀=10, h=10) with a cell load of 10 N and a head-speed of 0.5 mm/min. The data acquisition rate was set at 20 Hz. The compressive modulus was estimated as the slope of the linear region of the resulting stress–strain curves.

### 2.5.5 Differential Scanning Calorimetry (DSC)

Differential scanning calorimetric analyses were carried out using a Mettler Toledo DSC instrument. The measures were performed under nitrogen atmosphere (50 µl/min) setting a heating rate of 10 °C/min. Approximately 6 mg of each sample were sealed in a 100 µL aluminium pan with pierced lids.

### 2.5.6 Swelling Behaviour

The swelling behaviour was investigated by means of gravimetric analysis. The dried ~~hydrogels~~ OHGs (air drying) were first immersed in deionized water at RT. Then, the samples were removed from water at different time-intervals and subsequently weighted after removing the free water present on the surface with a filter paper. The swelling degree (SD%), the equilibrium swelling ratio ($S_{eq}$) and the equilibrium water content (EWC) were calculated with the following Equations (4,5,6).

$$SD\% = \left(\frac{W_t - W_d}{W_d}\right) * 100, \quad (4)$$

$$S_{eq} = \frac{W_e - W_d}{W_d} \quad (5)$$

$$EWC\% = \frac{W_e - W_d}{W_e} * 100, \quad (6)$$

where ~~$W_f$~~ $W_t$ is the ~~final~~ weight at time t, $W_d$ is the weight of the dry sample, and $W_e$ is the weight of the sample at the equilibrium state.

### 2.5.7 Field Emission Scanning Electron Microscopy (FESEM)

The morphological characterization of the ~~hydrogels~~OHGs was performed by using a FESEM Zeiss Supra 40 (Oberkochen, Germany). The sample were first lyophilized and then immersed in liquid nitrogen to induce a fragile fracture. Subsequently, the broken specimens were covered with a 5 nm thick film of Platinum.

### 2.5.8 Adsorption study

The adsorption study of MB was conducted by adding 8 mL of MB solution (40 mg/L) to 8 mg of dried ~~hydrogel~~OHG at T = 25 °C. Afterwards the vials were protected from light with an aluminium foil to avoid photocatalytic degradation of the dye. Then, fixed amount of supernatant was taken out at different time-intervals to monitor the dye adsorption. The MB concentration was determined by JENWAY 6850 UV/Vis (Cole-Parmer, Stone, Staffordshire, UK) UV-visible spectroscopy by following the peak centred at 665 nm. The adsorption capacity at time t ($q_m$ [mg/g]) and the equilibrium adsorption capacity ($q_e$ [mg/g]) were calculated according to Equations 7 and 8, respectively.

$$q_m = \frac{(C_0 - C_t) * V}{W} \quad (7)$$

$$q_e = \frac{(C_0 - C_e) * V}{W} \quad (8)$$

Where $C_0$ (mg/L) is the initial MB concentration, while $C_e$ (mg/L) and $C_t$ (mg/L) are the MB concentration at time t and at equilibrium, respectively. V (mL) is the volume of MB solution and W (g) is the mass of the dried ~~hydrogel~~OHG.

Two different kinetic models were then used to evaluate the adsorption rate and the potential rate controlling step. The kinetic data were analysed by means of pseudo-first order and pseudo-second order models [55], using the Lagergren Equations (9 and 10).

$$\frac{dq}{dt} = k_1(q_e - q_m) \quad (9)$$

$$-\ln\left(\frac{1-q_m}{q_e}\right) = k_1 t \quad (10)$$

where $k_1$ is the rate constant of pseudo-first order sorption [1/min]. According to this approximation, a plot of $-\ln((1-q)/q_e)$ vs t gives a straight line with slope $k_1$.

Equations 11 and 12 report the second-order kinetic rate equation and its integrated formula respectively [56].

$$\frac{dq}{dt} = k_2(q_e - q)^2 \quad (11)$$

$$\frac{t}{q} = \frac{1}{k_2 q_e^2} + \frac{t}{q_e} \quad (12)$$

where $k_2$ is the rate constant of the pseudo second order sorption [g/(mg min)]. According to this approximation, a plot of t/q vs t gives a linear relationship with slope $1/q_e$ and intercept $1/k_2q_e^2$.

### 2.5.9 Digital light processing (DLP) 3D-printing

The printability of the precursor formulations by means of DLP 3D – Printing was investigated using an Asiga UV-MAX DLP printer (nominal XY pixel resolution of 27 µm, light emission at λ=385nm). Different CAD models were converted into STL files and 3D printed. The layer thickness and the light intensity were fixed at 50 µm and 30 mW/cm$^2$, while the exposure time was ~~set at 3~~ ranged between 2.5 and 3 s, depending on the photocurable formulation being used. The printed objects were post-cured for 3 min using a mercury lamp provided by Robot Factory (UV-light, 12 mW/cm$^2$, 385 nm).

## 3. RESULTS AND DISCUSSION

Biorenewable photopolymerized "all-starch" ~~hydrogels~~OHGs were prepared from functionalized starch and γ-cyclodextrin, a starch derivative, and tested as bio-adsorbent for the removal of methylene blue from water. Both of the polysaccharides were functionalized *via* hydroxyl groups substitution to get derivatives suitable for photopolymerization processes. Accordingly, methacrylated starch (MS) and acrylated γ-cyclodextrin (ACy) were prepared

following two synthetic routes already reported in previous studies, using methacrylic anhydride and acryloyl chloride as functionalizing agents (Scheme 1) [51,52]. The complete procedures are given in the experimental section.

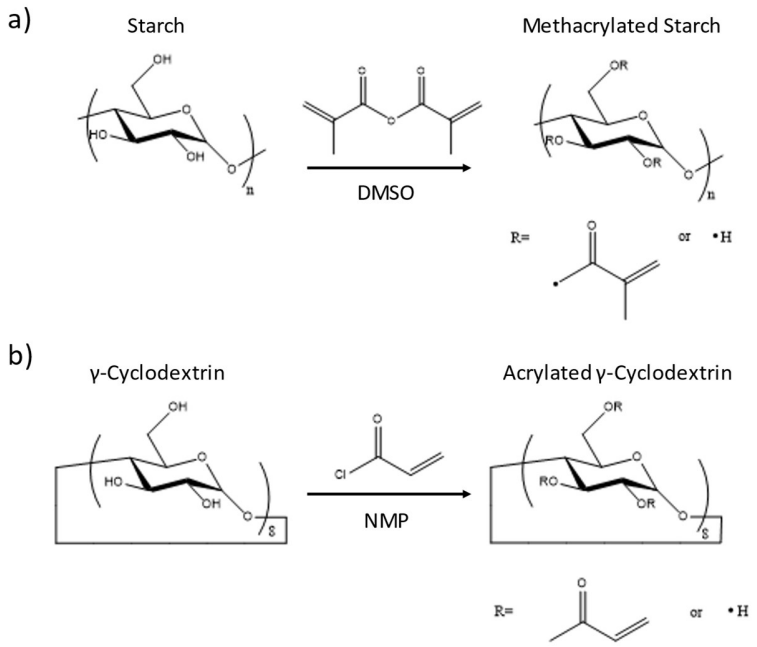


**Scheme 1**. Schematic representation of a) starch and b) cyclodextrin functionalization reactions.

The successful functionalizations were confirmed by means of $^{1}H$ NMR and $^{13}C\{^{1}H\}$ NMR, which revealed the typical signals of the new vinyl protons ($\delta^{1}H_{MS}$ = 5.66 and 6.07 ppm; $\delta^{1}H_{ACy}$ = 5.95, 6.18, and 6.32 ppm) and carbons ($\delta^{13}C_{MS}$ = 127.75 and 136.61 ppm; $\delta^{13}C_{ACy}$ = 128.39 and 132.06 ppm); methyl protons and carbons ($\delta^{1}H_{MS}$ = 1.9 ppm; $\delta^{13}C_{MS}$ = 18.45 ppm) and carbonyl carbons ($\delta^{13}C_{MS}$ = 170.38 ppm; $\delta^{13}C_{ACy}$ = 165.57 ppm) of the photoreactive derivatives MS (Fig. S1, Fig. S2) and ACy (Fig. S3, Fig. S4). The obtained degree of substitution (DOS) for

the hydroxyl groups were approximately 0.08 for MS and 0.9 for ACy in accordance ~~to~~with what was reported previously [51,52].

The efficiency of the functionalization was further proven by infrared spectroscopy. The ATR-FTIR spectra of MS and ACy were collected and compared to the spectra of the starting materials. The detailed assignment of the signals corresponding to the spectral vibrations of both the main polysaccharides groups and the new chemical functionalities is highlighted in Fig. 1 [57-59].

The new characteristic peaks corresponding to the C=$CH_2$ out of plane bending vibrations and C=O stretching vibration of meth-/acrylates can be easily observed at 815, 1640 $cm^{-1}$ and 1710 $cm^{-1}$, respectively [60-62]. The reduction of the intensity of the signal corresponding to the -OH vibration at 3340 $cm^{-1}$ further confirms the conversion of hydroxyl groups into (meth)acrylated functions of both starch and γ-cyclodextrin. Note that the reduction of the -OH peak intensity is more pronounced in the spectrum of acrylated ACy, ~~suggesting~~ confirming ~~a~~ the higher degree of functionalization [52].

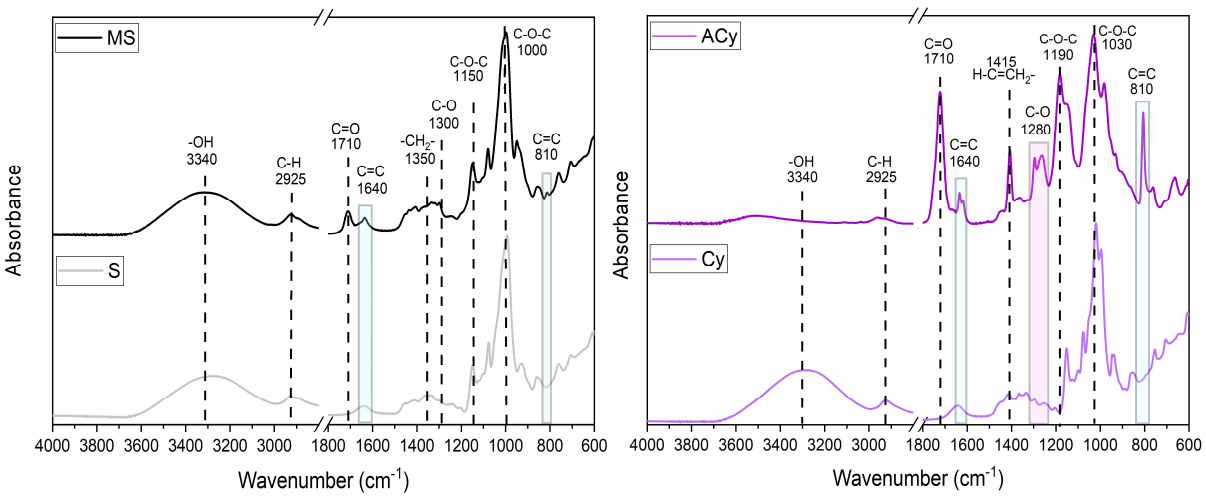

289 **Figure 1.** FTIR spectra of pristine Starch (S), γ-cyclodextrin (Cy) and their corresponding
290 methacrylated derivatives starch (MS) and acrylated γ-cyclodextrin (ACy).
291

292 Several photocurable formulations were prepared by dissolving different amounts of MS and
293 ACy in a $H_2O$/DMSO (20/80) mixture, while phenylbis(2,4,6-trimethylbenzoyl)phosphine oxide
294 (BAPO, registered trade name Omnicure 819) was added as a photoinitiator. DMSO was used as
295 co-solvent in order to increase the solubility of ACy in aqueous formulations. The chemical
296 composition of the final precursor formulations is given in the experimental section.

297 The photoreactivity of the formulations was evaluated by means of real-time photorheology. The
298 build-up of the polymer network was monitored by following the storage modulus (G') evolution
299 during UV-light irradiation. The photorheology curves shown in Figure 2a reveal the high
300 reactivity of these polysaccharides-based formulations. The induction time, i.e. the minimum time
301 required to start the photo-induced chemical crosslinking, is less than 2" for all investigated
302 formulations. Moreover, photo-crosslinking is completed within approximately 60", as confirmed
303 by the onset of the plateau value of the storage moduli (G'). However, even if all formulations
304 seem to have similar curing kinetics, as suggested by the similar slopes ($\Delta G'/\Delta t$) of the curves, the
305 reaction rates increase almost three times (from 134 to 335 Pa/s) as the concentration of ACy is
306 increased in the precursor formulation (see entry 1, Tab. 2). Also, higher G' values are reached
307 with increasing ACy content (see entry 2 Tab. 2). This proves that the addition of ACy into the
308 formulations leads to faster curing kinetics, due to the higher reactivity of acrylates with respect
309 to methacrylate moieties and the higher degree of functionalization of ACy. The higher
310 crosslinking efficiency of the cyclodextrin derivatives also generated stiffer hydrogels [52].

The viscoelastic properties of the ~~hydrogels~~ OHGs just formed upon UV-light irradiation were investigated by means of frequency sweep experiments. The dynamic viscosity $|\eta^*|$ and the storage modulus G' values are reported in Tab. 2. The $|\eta^*|$ slope values are approximately -0.9 for all the samples, suggesting a pseudo-plastic behaviour (Fig. 2b) [54]. Furthermore, performing the analysis in the linear viscoelastic region, it is possible to determine the network parameters in non-intrusive way, from the G' measured values [63].

The molar mass ($M_e^*$) and the distance ($\xi$) between two entanglements points decreased with increasing ACy content and the crosslink density ($v_e$) increased by more than an order of magnitude (see entries 3, 4 and 5, Table 2). These results are consistent with the high crosslinking efficiency of ACy [52]. The influence of ACy on the final properties of the UV-cured thermosetting networks was further confirmed by the thermo-mechanical characterizations that were carried out on dried samples. DSC measurements revealed an increase in the glass transition temperatures ($T_g$) with increasing amount of ACy in the precursor formulations, given that the increase in the crosslinking density of a polymer reflects into higher $T_g$ values (Tab. 2) [64]. Furthermore, the mechanical properties of the hydrogels were evaluated by means of compression tests. The obtained stress-strain curves are shown in Fig. 2c, while the Young's modulus ($E_c$), ~~and~~ the ultimate compression strength (UCS) ~~values~~ and compression at break are reported in Tab. 2. The $E_c$ values range from 0.78 to 3.93 MPa and are higher than the ones of other polysaccharides-based hydrogels already reported in the literature [65-67]. Once again, the higher the ACy content, the higher are both $E_c$ and UCS, meaning that the presence of ACy improved the mechanical performance of the photopolymerized networks as a result of the higher $v_e$ values. Whereas the compression at break slightly decreases in the presence of ACy, as expected for more crosslinked networks.

Subsequently, the water-absorption capability of these polysaccharide-based OHGs~~hydrogels~~ was investigated. First, the cured ~~hydrogels~~OHGs were immersed in water to remove DMSO *via* solvent exchange. Then, the samples were dried and immersed again in water to evaluate the degree of swelling at different time-intervals, following the procedure reported in the experimental section. The swelling kinetics of the ~~hydrogels~~ OHGs are shown in Figure 2d and the swelling at equilibrium ($S_{eq}$) and the equilibrium water content (EWC) values are listed in Tab. ~~3~~2. As displayed, all the photocured ~~hydrogels~~ OHGs reach $S_{eq}$ after approximately 15 hours. However, as expected from the crosslinking degree values, the presence of ACy affects the swelling degree, since both $S_{eq}$ and EWC decrease (from 395 to 54 and from 80 to 35, respectively) as the ACy content increases.

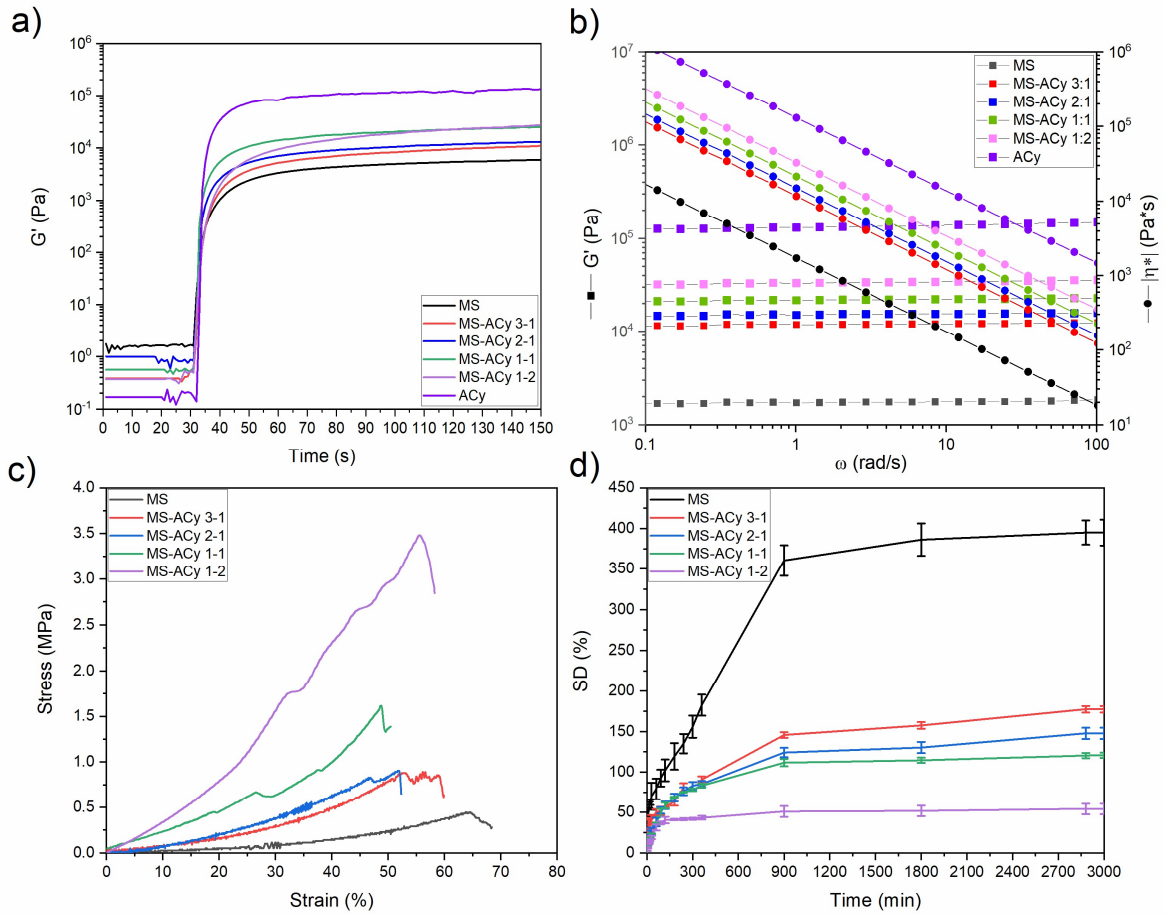

**Figure 2.** a) Photorheology curves; b) frequency sweep plots; c) stress-strain curves and d) swelling kinetic of the samples prepared from all the precursor formulations.

**Table 2.** Photo-/rheological, mechanical, thermal and swelling data of the MS-ACy organo/hydrogels.

| | MS | MS-Acy 3-1 | MS-Acy 2-1 | MS-Acy 1-1 | MS-Acy 1-2 | ACy |
|---|---|---|---|---|---|---|
| **Reaction rate [Pa/s]** | 134 | 201 | 266 | 300 | 335 | 1800 |
| **$G'_p$ [kPa]** | 1.8 | 12.0 | 15.4 | 22.1 | 34.1 | 131.2 |
| **$M_E$*[g/Mol]** | 156.5 | 22.9 | 17.9 | 12.5 | 8.1 | 2.1 |
| **$\nu_E$ [1/m$^3$]** | $4.3*10^{23}$ | $2.9*10^{24}$ | $3.7*10^{24}$ | $5.4*10^{24}$ | $8.3*10^{24}$ | $3.2*10^{25}$ |
| **$\xi$ [m]** | $1.3*10^{-8}$ | $7.0*10^{-9}$ | $6.4*10^{-9}$ | $5.7*10^{-9}$ | $4.9*10^{-9}$ | $3.1*10^{-9}$ |
| **$T_G$ [°C]** | 95 | 98 | 100 | 102 | 109 | N.A. |
| **$E_C$ [MPa]** | 0.36±0.15 | 0.78±0.01 | 1.04±0.08 | 2.10±0.28 | 3.93±0.11 | N.A. |
| **Compression at break [%]** | 64±2.3 | 56±4.0 | 52±0.1 | 49±2.8 | 56±3.5 | N.A. |
| **UCS [MPa]** | 0.59±0.19 | 0.89±0.10 | 0.90±0.13 | 1.62±0.15 | 3.48±0.23 | N.A. |
| **$S_{EQ}$** | 3.95±0.15 | 1.78±0.04 | 1.47±0.07 | 1.2±0.03 | 0.54±0.06 | N.A. |
| **EWC [%]** | 80±0.7 | 64±0.9 | 60±1.4 | 55±1.0 | 35±2.7 | N.A. |

$M_e$* molar mass between two entablements points, $\xi$ distance between two entanglements points, $\nu_e$ ~~crosslinking density~~numbers of crosslinks, $E_c$ Young's modulus, UCS ultimate compression strength, $S_{eq}$ swelling at equilibrium and EWC equilibrium water content.

The effect of ACy on the ~~hydrogel~~ OHG structure was further proved by the microstructural characterization. The FESEM images of the different ~~hydrogels~~ OHGs are shown in Figure 3 (higher magnification available in Figure 5S). The structure of the ~~hydrogels~~ OHGs prepared from MS is highly porous, with pore size even higher than 20 µm (Fig. 3a). Instead, the addition of ACy in the photocurable formulations leads to a reduction of the porosity. As displayed in Fig. 3b-e, both the pore number and size decreased with the increasing ACy content. The microstructure of a sample prepared from 100% ACy is given for comparison in Fig. 3f. As you can see, this last sample does not present any porosity, at least not in the micrometric scale. These results are in

good agreement with the previous findings, further confirming that the addition of ACy leads to higher crosslinking density (higher $v_e$) with lower $M_e$* and ξ.

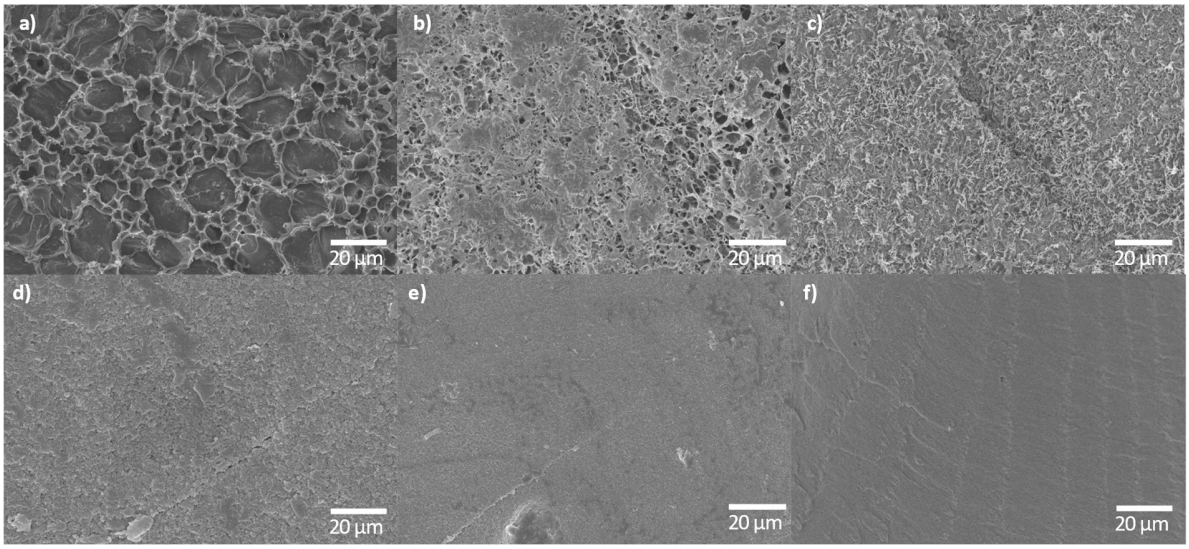


**Figure 3.** FESEM images of different samples prepared from a) MS, b) MS-ACy 3-1, c) MS-ACy 2-1,d) MS-ACy 1-1, e) MS-ACy 1-2, f) ACy.

Finally, the photocured ~~hydrogels~~ OHGs were tested as adsorbent materials for the removal of organic dyes from water. The chelating properties of the hydroxyl groups of starch make these ~~hydrogels~~ OHGs especially promising candidates for the removal of cationic dyes. Moreover, the presence of cyclodextrins within the structure of the polymeric network can increase the absorption capability due to the ability of cyclodextrins to form host-guest inclusion complexes. Methylene blue (MB) was selected as a model dye molecule, due to its fit to the dimension of the cavity of γ-cyclodextrin that enables efficient complexation [68]. The MB adsorption kinetics are displayed in Fig. 4.

As shown in Fig. 4a, the MB adsorption proceeded rapidly reaching a plateau after about 100 min ($q_e$). The obtained $q_e$ values are in good agreement with the ones reported in the literature for other polysaccharides-based hydrogels, such as those prepared with carboxymethyl cellulose/graphene oxide (GO) (59 mg/g) [69], regenerated cellulose/GO [70], corn stalk/organic montmorillonite composite (49 mg/g) [71] and carbonized lignosulfonate/gelatin (38 mg/g) [72].

The adsorption of cationic dyes into polysaccharides-based hydrogels mainly depends on the hydrogel composition, since the absorption is mainly affected by the generation of hydrogen bonds between the hydroxyl groups of the polymer chains and the amide group of the dye molecule. Moreover, the absorption is also affected by the porosity of the network. Therefore, the increase of the crosslinking density lowers the free volume and the dye absorption is expected to decrease accordingly [60].

But on the contrary, the relative amount of MB absorbed into our MS-ACy ~~hydrogels~~ OHGs increased with the increase of $v_e$ and the reduction of network porosity. As shown in Table 3, the $q_e$ of the ~~hydrogels~~ OHGs increased from 42 to 59 mg/g with increasing content of ACy, reaching a maximum of +50 wt% with respect to the samples prepared from 100% MS. However, if the ACy content was furtherly increased the $q_e$ seems indeed to be negatively affected. The maximum absorption capability is reached by keeping the ratio MS:ACy at 1:1 and the 50 wt% of ACy might represent a threshold beyond which the molecular diffusion into the network is hindered by the $v_e$ enhancement, resulting into a lower absorption. The higher absorption values reached with the less porous and more crosslinked ~~hydrogels~~ OHGs which show a lowered swelling capability can be explained simply by the increased number of ACy units which seemingly remain accessible and therefore lead to an increased number of host-guest inclusion complexes between MB and γ-cyclodextrin [68]. Therefore, the absorption of MB

likely occurs following two different mechanisms: a) H-bonding interactions between the residual -OH groups of MS and ACy and b) MB complexation into the cavity of ACy.

The adsorption rates ($k_a$) were also estimated by evaluating the slopes of the first linear part of the curves [60]. The high $k_a$ values obtained with an increase from 0.49 to 0.81 [mg/(g*s)] with increasing ACy content, (Table 34) suggest that the adsorption mainly occurred on the hydrogel surface. This finding is consistent with the absorption evolution scaling with time, since the $q_e$ of the ~~hydrogels~~ OHGs is reached within the first 100 min, a time much shorter than required to reach the swelling equilibrium (15 hours).

The absorption data were then fitted using pseudo-first-order and pseudo-second-order models. Fig. 4c-d show the results of the fitting analyses. As can be seen from the graph reported in Fig. 4c, the experimental data do not fit with the linear trend expected from the pseudo-first-order model which is therefore not applicable ~~the pseudo-first-order model is not applicable, since there is no linear correlation between the experimental and the calculated data~~ [55]. On the contrary, the pseudo-second-order model correctly describes the MB adsorption into the MS-ACy ~~hydrogels~~OHGs, as confirmed by the high correlation coefficient $R^2$ (>0.99823) and the calculated absorption capacity ($q_{e,calc}$) values that fit with the experimental data ($q_{e,exp}$). All the data resulting from the pseudo-second-order fitting are listed in Table 3. The excellent data fitting with the pseudo-second-order kinetic model suggests that the rate-determining step is chemisorption [73].

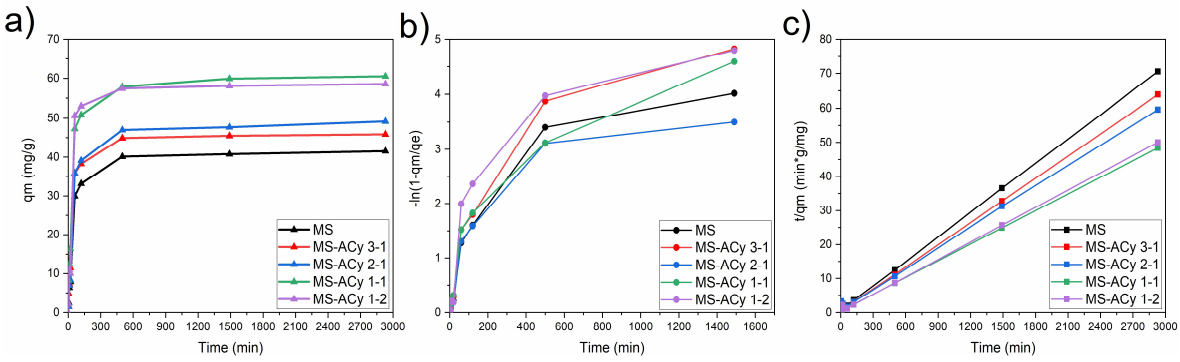


**Figure 4.** a) $q_m$ vs time, b) data fitted using the pseudo-first order kinetic model, c~~b~~) data fitted using the pseudo-second-order kinetic model for the absorption of MB into the different MS-ACy ~~hydrogels~~OHGs.

**Table 3.** Pseudo-second-order fitting parameters for MB adsorption.

| Sample | $k_a$ [mg/(g*s)] | $q_{e,\,calc}$ [mg/g] | $q_{e,\,exp}$ [mg/g] | $k_2$ [g/(mg*min)] | $R^2$ |
|---|---|---|---|---|---|
| **MS** | 0.49 | 41.52 | 42.30 | $4.52*10^{-4}$ | 0.999525 |
| **MS-ACy 3-1** | 0.58 | 45.83 | 46.49 | $5.82*10^{-4}$ | 0.999771 |
| **MS-ACy 2-1** | 0.60 | 49.17 | 50.40 | $2.75*10^{-4}$ | 0.998231 |
| **MS-ACy 1-1** | 0.80 | 60.53 | 59.88 | $3.08*10^{-4}$ | 0.997972 |
| **MS-ACy 1-2** | 0.81 | 58.55 | 61.24 | $4.95*10^{-4}$ | 0.996524 |

~~Based on these results of the good reactivity of the investigated formulations towards UV light initiated photopolymerization, the DLP printability of the most promising formulation with respect to the absorption capacity was assessed. As shown in Figure 5, free standing 3D printed geometries were successfully obtained with a good resolution without the use of any additional dyes during the printing process. This is an interesting preliminary result, as the good DLP-printability will allow the design of photocured hydrogels with complex geometries to suit specific applications and to improve the adsorption properties by increasing the surface area of the hydrogels, which will enhance the process of chemisorption~~

Based on the good reactivity of the formulations towards UV-light initiated photopolymerization (i.e. short induction times and fast curing kinetic), the DLP-printability was assessed, focusing in particular on the two formulations having the best adsorption properties (MS-ACy 1-1 and MS-ACy 1-2). First the printability was investigated without using any additional dye. The preliminary results showed that even though both the formulations can be successfully 3D-printed, the final resolution of the printed objects was quite low due to over-polymerization (Fig. 5a - top), especially for those structures having small-scale details (see Fig. S6). Therefore, methyl red (MR) was added as dye to limit light-diffusion in the vat while printing. The MR concentration was set at 0.2 phr since this content doesn't affect significantly the photopolymerization kinetic (see Figure S7) but is enough to improve considerably the printing resolution (Figure 5a - bottom). However, the structures prepared from MS-ACy 1-1 showed poor self-standing properties. To improve the mechanical stability, further 3D-printing investigations were carried out by using MS-ACy 1-2, given that the higher content of ACy leads to more crosslinked and stiffer samples. As shown in Figure 5b-c, different objects were successfully printed with a good fidelity to the digital CAD models and a higher mechanical stability. This is an interesting preliminary result, as the good DLP-printability will allow the design of complex geometries with high surface area would improve the adsorption properties of the material by enhancing the chemisorption process.

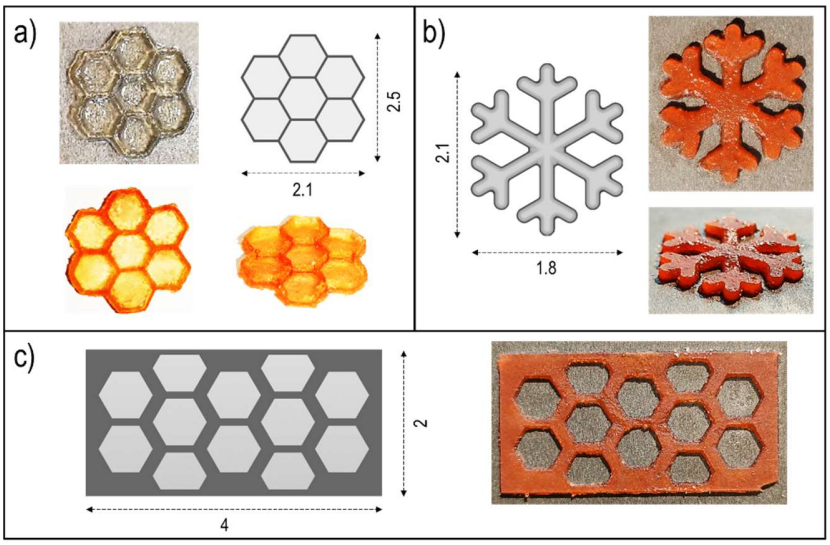


**Figure 5**: DLP-printed organo/hydrogels from a) MS-ACy 1-1 and b-c) MS-ACy 1-2.

## 4. CONCLUSIONS

Novel polysaccharide-based photocurable ~~hydrogels~~ organo/hydrogels were fabricated *via* UV-curing of photoreactive starch and γ-cyclodextrin derivatives and tested as bio-absorbents for the removal of methylene blue from water. Methacrylated starch (MS) and acrylated γ-cyclodextrin (ACy) were successfully synthetized to be exploited in photocuring processes and the real-time photorheology analysis revealed that increasing the ACy content fastens the kinetics due to the high reactivity of the multi-acrylated macromer. Rheological, thermo-mechanical and morphological tests performed on the photocrosslinked hydrogels revealed that higher amounts of ACy lead to an increase of the cross-link density, with the formation of stiffer networks with smaller porosity. Besides fastening the photopolymerization kinetic and stiffening the resulting ~~hydrogel~~ networks, ACy had a strong influence on the absorption capabilities of the ~~hydrogels~~OHGs. The results of the swelling and absorption tests revealed that the final properties

of the ~~hydrogels~~ OHGs could be easily tailored by modulating the ingredients within the precursor formulations. In fact, even if the swelling equilibrium values decreased, higher MB absorption capacity was recorded with the increase of ACy content ~~into the hydrogel~~, possibly due to the combination of the chelating properties of the hydroxyl groups of MS and the ability of ACy to form inclusion complexes with MB. All the ~~HS~~ absorption experimental data correctly fitted with the pseudo-second-order kinetic model, suggesting chemical adsorption. Furthermore, the DLP printability of these polysaccharides-based ~~hydrogels~~ OHGs was demonstrated, opening a new frontier for wastewater treatment.

## AUTHOR INFORMATION

### Corresponding Author

*Marco Sangermano. DISAT, Politecnico di Torino, Corso Duca degli Abruzzi 21, 10129 Torino, Italy, Email: marco.sangermano@polito.it

### Author Contributions

The manuscript was written through contributions of all authors. All authors have given approval to the final version of the manuscript.

### Funding Sources

This project was partially founded from the European Union's Horizon 2020 research and innovation program under the Marie Skłodowska-Curie [grant agreement No 101007578]

## ABBREVIATIONS

S Starch, MS Methacrylated Starch, C γ-Cyclodextrin, AC Acrylated γ-Cyclodextrin.

## REFERENCES


[1] M.A. Hassaan, A. el Nemr, Health and Environmental Impacts of Dyes : Mini Review, American Journal of Environmental Science and Engineering. 1 (2017) 64–67. https://doi.org/10.11648/j.ajese.20170103.11.

[2] F. Rafii, W. Franklin, C.E. Cerniglia, Azoreductase activity of anaerobic bacteria isolated from human intestinal microflora, Applied and Environmental Microbiology. 56 (1990) 2146–2151. https://doi.org/10.1128/aem.56.7.2146-2151.1990.

[3] H. Ali, Biodegradation of synthetic dyes - A review, Water, Air, and Soil Pollution. 213 (2010) 251–273. https://doi.org/10.1007/s11270-010-0382-4.

[4] D.C. Kalyani, A.A. Telke, R.S. Dhanve, J.P. Jadhav, Ecofriendly biodegradation and detoxification of Reactive Red 2 textile dye by newly isolated Pseudomonas sp. SUK1, Journal of Hazardous Materials. 163 (2009) 735–742. https://doi.org/10.1016/j.jhazmat.2008.07.020.

[5] S. Rodríguez Couto, Dye removal by immobilised fungi, Biotechnology Advances. 27 (2009) 227–235. https://doi.org/10.1016/j.biotechadv.2008.12.001.

[6] I.M. Banat, P. Nigam, D. Singh, R. Marchant, Microbial decolorization of textile-dye-containing effluents: A review, Bioresource Technology. 58 (1996) 217–227. https://doi.org/10.1016/S0960-8524(96)00113-7.

[7] G. Jing, L. Wang, H. Yu, W.A. Amer, L. Zhang, Recent progress on study of hybrid hydrogels for water treatment, Colloids and Surfaces A: Physicochemical and Engineering Aspects. 416 (2013) 86–94. https://doi.org/10.1016/j.colsurfa.2012.09.043.

[8] S. Chatterjee, A. Kumar, S. Basu, S. Dutta, Application of Response Surface Methodology for Methylene Blue dye removal from aqueous solution using low cost adsorbent, Chemical Engineering Journal. 181–182 (2012) 289–299. https://doi.org/10.1016/j.cej.2011.11.081.

[9] D. Sarmah, N. Karak, Double network hydrophobic starch based amphoteric hydrogel as an effective adsorbent for both cationic and anionic dyes, Carbohydrate Polymers. 242 (2020) 116320. https://doi.org/10.1016/j.carbpol.2020.116320.

[10] Y. Fu, T. Viraraghavan, Fungal decolorization of dye wastewaters: A review, Bioresource Technology. 79 (2001) 251–262. https://doi.org/10.1016/S0960-8524(01)00028-1.

[11] L. Meng, X. Zhang, Y. Tang, K. Su, J. Kong, Hierarchically porous silicon–carbon–nitrogen hybrid materials towards highly efficient and selective adsorption of organic dyes, Scientific Reports. 5 (2015) 7910. https://doi.org/10.1038/srep07910.

519 [12] Z. Zhao, L. Li, G.S. Geleta, L. Ma, Z. Wang, Polyacrylamide-Phytic Acid-Polydopamine
520 Conducting Porous Hydrogel for Efficient Removal of Water-Soluble Dyes, Scientific Reports. 7
521 (2017) 1–10. https://doi.org/10.1038/s41598-017-08220-6.

522 [13] V. Sinha, S. Chakma, Advances in the preparation of hydrogel for wastewater treatment:
523 A concise review, Journal of Environmental Chemical Engineering. 7 (2019) 103295.
524 https://doi.org/10.1016/j.jece.2019.103295.

525 [14] B. Mandal, S.K. Ray, Synthesis of interpenetrating network hydrogel from poly(acrylic
526 acid-co-hydroxyethyl methacrylate) and sodium alginate: Modeling and kinetics study for
527 removal of synthetic dyes from water, Carbohydrate Polymers. 98 (2013) 257–269.
528 https://doi.org/10.1016/j.carbpol.2013.05.093.

529 [15] Q. Lv, Y. Shen, Y. Qiu, M. Wu, L. Wang, Poly(acrylic acid)/poly(acrylamide) hydrogel
530 adsorbent for removing methylene blue, Journal of Applied Polymer Science. 137 (2020) 1–9.
531 https://doi.org/10.1002/app.49322.

532 [16] A.T. Paulino, M.R. Guilherme, A. v. Reis, G.M. Campese, E.C. Muniz, J. Nozaki,
533 Removal of methylene blue dye from an aqueous media using superabsorbent hydrogel
534 supported on modified polysaccharide, Journal of Colloid and Interface Science. 301 (2006) 55–
535 62. https://doi.org/10.1016/j.jcis.2006.04.036.

536 [17] G. Melilli, J. Yao, A. Chiappone, M. Sangermano, M. Hakkarainen, Photocurable "all-
537 lignocellulose" derived hydrogel nanocomposites for adsorption of cationic contaminants,
538 Sustainable Materials and Technologies. 27 (2021).
539 https://doi.org/10.1016/j.susmat.2020.e00243.

540 [18] S. Kamel, A.A. El-Gendy, M.A. Hassan, M. El-Sakhawy, I. Kelnar, Carboxymethyl
541 cellulose-hydrogel embedded with modified magnetite nanoparticles and porous carbon:
542 Effective environmental adsorbent, Carbohydrate Polymers. 242 (2020).
543 https://doi.org/10.1016/j.carbpol.2020.116402.

544 [19] W. Wang, H. Bai, Y. Zhao, S. Kang, H. Yi, T. Zhang, S. Song, Synthesis of chitosan
545 cross-linked 3D network-structured hydrogel for methylene blue removal, International Journal
546 of Biological Macromolecules. 141 (2019) 98–107.
547 https://doi.org/10.1016/j.ijbiomac.2019.08.225.

548 [20] Z. Feng, K. Odelius, M. Hakkarainen, Tunable chitosan hydrogels for adsorption:
549 Property control by biobased modifiers, Carbohydrate Polymers. 196 (2018) 135–145.
550 https://doi.org/10.1016/j.carbpol.2018.05.029.

551 [21] A.C.N. de Azevedo, M.G. Vaz, R.F. Gomes, A.G.B. Pereira, A.R. Fajardo, F.H.A.
552 Rodrigues, Starch/rice husk ash based superabsorbent composite: high methylene blue removal
553 efficiency, Iranian Polymer Journal (English Edition). 26 (2017) 93–105.
554 https://doi.org/10.1007/s13726-016-0500-2.

555 [22] C.B. Godiya, Y. Xiao, X. Lu, Amine functionalized sodium alginate hydrogel for
556 efficient and rapid removal of methyl blue in water, International Journal of Biological
557 Macromolecules. 144 (2020) 671–681. https://doi.org/10.1016/j.ijbiomac.2019.12.139.

558 [23] M.S. Amini-Fazl, A. Ahmari, Dextran-graft-poly(hydroxyethyl methacrylate) biosorbents
559 for removal of dyes and metal cations, Materials Research Express. 6 (2019).
560 https://doi.org/10.1088/2053-1591/ab0072.

561 [24] M. Nasrollahzadeh, M. Sajjadi, S. Iravani, R.S. Varma, Starch, cellulose, pectin, gum,
562 alginate, chitin and chitosan derived (nano)materials for sustainable water treatment: A review,
563 Carbohydrate Polymers. 251 (2021) 116986. https://doi.org/10.1016/j.carbpol.2020.116986.

564 [25] D. Ma, B. Zhu, B. Cao, J. Wang, J. Zhang, Fabrication of the novel hydrogel based on
565 waste corn stalk for removal of methylene blue dye from aqueous solution, Applied Surface
566 Science. 422 (2017) 944–952. https://doi.org/10.1016/j.apsusc.2017.06.072.

567 [26] H. Kolya, A. Roy, T. Tripathy, Starch-g-Poly-(N, N-dimethyl acrylamide-co-acrylic
568 acid): An efficient Cr (VI) ion binder, International Journal of Biological Macromolecules. 72
569 (2014) 560–568. https://doi.org/10.1016/j.ijbiomac.2014.09.003.

570 [27] M.I. Khalil, S. Farag, Utilization of some starch derivatives in heavy metal ions removal,
571 Journal of Applied Polymer Science. 69 (1998) 45–50. https://doi.org/10.1002/(SICI)1097-
572 4628(19980705)69:1<45::AID-APP6>3.0.CO;2-M.

573 [28] Z. Li, M. Wang, F. Wang, Z. Gu, G. Du, J. Wu, J. Chen, γ-Cyclodextrin: A review on
574 enzymatic production and applications, Applied Microbiology and Biotechnology. 77 (2007)
575 245–255. https://doi.org/10.1007/s00253-007-1166-7.

576 [29] B. Tian, J. Liu, The classification and application of cyclodextrin polymers: a review,
577 New Journal of Chemistry. 44 (2020) 9137–9148. https://doi.org/10.1039/c9nj05844c.

578 [30] G. Liu, Q. Yuan, G. Hollett, W. Zhao, Y. Kang, J. Wu, Cyclodextrin-based host-guest
579 supramolecular hydrogel and its application in biomedical fields, Polymer Chemistry. 9 (2018)
580 3436–3449. https://doi.org/10.1039/c8py00730f.

581 [31] H.L. Jiang, J.C. Lin, W. Hai, H.W. Tan, Y.W. Luo, X.L. Xie, Y. Cao, F.A. He, A novel
582 crosslinked β-cyclodextrin-based polymer for removing methylene blue from water with high
583 efficiency, Colloids and Surfaces A: Physicochemical and Engineering Aspects. 560 (2019) 59–
584 68. https://doi.org/10.1016/j.colsurfa.2018.10.004.

585 [32] E. Renard, A. Deratani, G. Volet, B. Sebille, Preparation and characterization of water
586 soluble high molecular weight β-cyclodextrin-epichlorohydrin polymers, European Polymer
587 Journal. 33 (1997) 49–57. https://doi.org/10.1016/S0014-3057(96)00123-1.

588 [33] D. Landy, I. Mallard, A. Ponchel, E. Monflier, S. Fourmentin, Remediation technologies
589 using cyclodextrins: An overview, Environmental Chemistry Letters. 10 (2012) 225–237.
590 https://doi.org/10.1007/s10311-011-0351-1.

591 [34] B. Sancey, G. Trunfio, J. Charles, P.M. Badot, G. Crini, Sorption onto crosslinked
592 cyclodextrin polymers for industrial pollutants removal: An interesting environmental approach,
593 Journal of Inclusion Phenomena and Macrocyclic Chemistry. 70 (2011) 315–320.
594 https://doi.org/10.1007/s10847-010-9841-1.

595 [35] E.Y. Ozmen, M. Yilmaz, Use of β-cyclodextrin and starch based polymers for sorption of
596 Congo red from aqueous solutions, Journal of Hazardous Materials. 148 (2007) 303–310.
597 https://doi.org/10.1016/j.jhazmat.2007.02.042.

598 [36] G. Zhang, S. Shuang, C. Dong, J. Pan, Study on the interaction of methylene blue with
599 cyclodextrin derivatives by absorption and fluorescence spectroscopy, Spectrochimica Acta -
600 Part A: Molecular and Biomolecular Spectroscopy. 59 (2003) 2935–2941.
601 https://doi.org/10.1016/S1386-1425(03)00123-9.

602 [37] J. sheng Yang, S. ya Han, L. Yang, H. cheng Zheng, Synthesis of beta-cyclodextrin-
603 grafted-alginate and its application for removing methylene blue from water solution, Journal of
604 Chemical Technology and Biotechnology. 91 (2016) 618–623. https://doi.org/10.1002/jctb.4612.

605 [38] D. Kundu, S.K. Mondal, T. Banerjee, Development of β-Cyclodextrin-
606 Cellulose/Hemicellulose-Based Hydrogels for the Removal of Cd(II) and Ni(II): Synthesis,
607 Kinetics, and Adsorption Aspects, Journal of Chemical and Engineering Data. 64 (2019) 2601–
608 2617. https://doi.org/10.1021/acs.jced.9b00088.

609 [39] Z. Hao, Z. Yi, C. Bowen, L. Yaxing, Z. Sheng, Preparing γ-cyclodextrin-immobilized
610 starch and the study of its removal properties to dyestuff from wastewater, Polish Journal of
611 Environmental Studies. 28 (2019) 1701–1711. https://doi.org/10.15244/pjoes/90028.

612 [40] C.Y. Chen, C.C. Chen, Y.C. Chung, Removal of phthalate esters by α-cyclodextrin-
613 linked chitosan bead, Bioresource Technology. 98 (2007) 2578–2583.
614 https://doi.org/10.1016/j.biortech.2006.09.009.

615 [41] T. Tojima, H. Katsura, M. Nishiki, N. Nishi, S. Tokura, N. Sakairi, Chitosan beads with
616 pendant α-cyclodextrin: Preparation and inclusion property to nitrophenolates, Carbohydrate
617 Polymers. 40 (1999) 17–22. https://doi.org/10.1016/S0144-8617(99)00030-2.

618 [42] L. Fan, Y. Zhang, C. Luo, F. Lu, H. Qiu, M. Sun, Synthesis and characterization of
619 magnetic β-cyclodextrin-chitosan nanoparticles as nano-adsorbents for removal of methyl blue,
620 International Journal of Biological Macromolecules. 50 (2012) 444–450.
621 https://doi.org/10.1016/j.ijbiomac.2011.12.016.

622 [43] B. Martel, M. Devassine, G. Crini, M. Weltrowski, M. Bourdonneau, M. Morcellet,
623 Preparation and sorption properties of a β-cyclodextrin-linked chitosan derivative, Journal of
624 Polymer Science, Part A: Polymer Chemistry. 39 (2001) 169–176. https://doi.org/10.1002/1099-
625 0518(20010101)39:1<169::AID-POLA190>3.0.CO;2-G.

626 [44] T.F. Cova, D. Murtinho, R. Aguado, A.A.C.C. Pais, A.J.M. Valente, Cyclodextrin
627 Polymers and Cyclodextrin-Containing Polysaccharides for Water Remediation,
628 Polysaccharides. 2 (2021) 16–38. https://doi.org/10.3390/polysaccharides2010002.

[45] M. Fırlak, M.V. Kahraman, E.K. Yetimoğlu, Preparation and characterization of photocured thiol-ene hydrogel: Adsorption of Au(III) ions from aqueous solutions, Journal of Applied Polymer Science. 126 (2012) 322–332. https://doi.org/10.1002/app.36887.

[46] S. Zhao, F. Zhou, L. Li, M. Cao, D. Zuo, H. Liu, Removal of anionic dyes from aqueous solutions by adsorption of chitosan-based semi-IPN hydrogel composites, Composites Part B: Engineering. 43 (2012) 1570–1578. https://doi.org/10.1016/j.compositesb.2012.01.015.

[47] M. Firlak, M.V. Kahraman, E.K. Yetimoğlu, B. Zeytuncu, Adsorption of Ag (I) Ions from Aqueous Solutions Using Photocured Thiol-Ene Hydrogel, Separation Science and Technology (Philadelphia). 48 (2013) 2860–2870. https://doi.org/10.1080/01496395.2013.811692.

[48] G. Melilli, J. Yao, A. Chiappone, M. Sangermano, M. Hakkarainen, Photocurable "all-lignocellulose" derived hydrogel nanocomposites for adsorption of cationic contaminants, Sustainable Materials and Technologies. 27 (2021). https://doi.org/10.1016/j.susmat.2020.e00243.

[49] M. Sangermano, I. Roppolo, M. Messori, UV-cured functional coatings, RSC Smart Materials. 2015 (2015) 121–133.

[50] M. Sangermano, I. Roppolo, A. Chiappone, New horizons in cationic photopolymerization, Polymers. 10 (2018). https://doi.org/10.3390/polym10020136.

[51] C. Noè, C. Tonda-Turo, A. Chiappone, M. Sangermano, M. Hakkarainen, Light processable starch hydrogels, Polymers. 12 (2020) 1359. https://doi.org/10.3390/POLYM12061359.

[52] A. Cosola, R. Conti, H. Grützmacher, M. Sangermano, I. Roppolo, C.F. Pirri, A. Chiappone, Multiacrylated Cyclodextrin: A Bio-Derived Photocurable Macromer for VAT 3D Printing, Macromolecular Materials and Engineering. 305 (2020) 1–6. https://doi.org/10.1002/mame.202000350.

[53] G.A. Appuhamillage, D.R. Berry, C.E. Benjamin, M.A. Luzuriaga, J.C. Reagan, J.J. Gassensmith, R.A. Smaldone, A biopolymer-based 3D printable hydrogel for toxic metal adsorption from water, Polymer International. 68 (2019) 964–971. https://doi.org/10.1002/pi.5787.

[54] O.S. Lawal, J. Storz, H. Storz, D. Lohmann, D. Lechner, W.M. Kulicke, Hydrogels based on carboxymethyl cassava starch cross-linked with di- or polyfunctional carboxylic acids: Synthesis, water absorbent behavior and rheological characterizations, European Polymer Journal. 45 (2009) 3399–3408. https://doi.org/10.1016/j.eurpolymj.2009.09.019.

[55] M.T. Uddin, M.A. Islam, S. Mahmud, M. Rukanuzzaman, Adsorptive removal of methylene blue by tea waste, Journal of Hazardous Materials. 164 (2009) 53–60. https://doi.org/10.1016/j.jhazmat.2008.07.131.

[56] Y.S. Ho, G. McKay, Pseudo-second order model for sorption processes, Process Biochemistry. 34 (1999) 451–465. https://doi.org/10.1016/S0032-9592(98)00112-5.

[57] R. Kizil, J. Irudayaraj, K. Seetharaman, Characterization of irradiated starches by using FT-Raman and FTIR spectroscopy, Journal of Agricultural and Food Chemistry. 50 (2002) 3912–3918. https://doi.org/10.1021/jf011652p.

[58] D. Wu, M. Hakkarainen, A closed-loop process from microwave-assisted hydrothermal degradation of starch to utilization of the obtained degradation products as starch plasticizers, ACS Sustainable Chemistry and Engineering. 2 (2014) 2172–2181. https://doi.org/10.1021/sc500355w.

[59] E.S. Gil, L. Wu, L. Xu, T.L. Lowe, B-Cyclodextrin-Poly(B-Amino Ester) Nanoparticles for Sustained Drug Delivery Across the Blood-Brain Barrier, Biomacromolecules. 13 (2012) 3533–3541. https://doi.org/10.1021/bm3008633.

[60] Y.S. Jeon, J. Lei, J.H. Kim, Dye adsorption characteristics of alginate/polyaspartate hydrogels, Journal of Industrial and Engineering Chemistry. 14 (2008) 726–731. https://doi.org/10.1016/j.jiec.2008.07.007.

[61] A. v Reis, M.R. Guilherme, T.A. Moia, L.H.C. Mattoso, E.C. Muniz, E.B. Tambourgi, Synthesis and characterization of a starch-modified hydrogel as potential carrier for drug delivery system, Journal of Polymer Science Part A: Polymer Chemistry. 46 (2008) 2567–2574. https://doi.org/10.1002/pola.22588.

[62] G. Bayramoglu, Methacrylated chitosan based UV curable support for enzyme immobilization, Materials Research. 20 (2017) 452–459. https://doi.org/10.1590/1980-5373-MR-2016-0789.

[63] C. Seidel, W.M. Kulicke, C. Heß, B. Hartmann, M.D. Lechner, W. Lazik, Influence of the cross-linking agent on the gel structure of starch derivatives, Starch/Staerke. 53 (2001) 305–310. https://doi.org/10.1002/1521-379X(200107)53:7<305::AID-STAR305>3.0.CO;2-Z.

[64] L.E. Nielsen, Cross-Linking–Effect on Physical Properties of Polymers, Journal of Macromolecular Science, Part C. 3 (1969) 69–103. https://doi.org/10.1080/15583726908545897.

[65] C. Ceccaldi, S.G. Fullana, C. Alfarano, O. Lairez, D. Calise, D. Cussac, A. Parini, B. Sallerin, Alginate scaffolds for mesenchymal stem cell cardiac therapy: Influence of alginate composition, Cell Transplantation. 21 (2012) 1969–1984. https://doi.org/10.3727/096368912X647252.

[66] G. Melilli, I. Carmagnola, C. Tonda-Turo, F. Pirri, G. Ciardelli, M. Sangermano, M. Hakkarainen, A. Chiappone, DLP 3D printing meets lignocellulosic biopolymers: Carboxymethyl cellulose inks for 3D biocompatible hydrogels, Polymers. 12 (2020) 1–11. https://doi.org/10.3390/POLYM12081655.

[67] M.Y. Shie, J.J. Lee, C.C. Ho, S.Y. Yen, H.Y. Ng, Y.W. Chen, Effects of gelatin methacrylate bio-ink concentration on mechano-physical properties and human dermal fibroblast behavior, Polymers. 12 (2020) 1–18. https://doi.org/10.3390/POLYM12091930.

[68] Z. Hao, Z. Yi, C. Bowen, L. Yaxing, Z. Sheng, Preparing γ-cyclodextrin-immobilized starch and the study of its removal properties to dyestuff from wastewater, Polish Journal of Environmental Studies. 28 (2019) 1701–1711. https://doi.org/10.15244/pjoes/90028.

[69] J. Liu, H. Chu, H. Wei, H. Zhu, G. Wang, J. Zhu, J. He, Facile fabrication of carboxymethyl cellulose sodium/graphene oxide hydrogel microparticles for water purification, RSC Advances. 6 (2016) 50061–50069. https://doi.org/10.1039/c6ra06438h.

[70] F. Ren, Z. Li, W.Z. Tan, X.H. Liu, Z.F. Sun, P.G. Ren, D.X. Yan, Facile preparation of 3D regenerated cellulose/graphene oxide composite aerogel with high-efficiency adsorption towards methylene blue, Journal of Colloid and Interface Science. 532 (2018) 58–67. https://doi.org/10.1016/j.jcis.2018.07.101.

[71] D. Ma, B. Zhu, B. Cao, J. Wang, J. Zhang, Fabrication of the novel hydrogel based on waste corn stalk for removal of methylene blue dye from aqueous solution, Applied Surface Science. 422 (2017) 944–952. https://doi.org/10.1016/j.apsusc.2017.06.072.

[72] J. Yao, K. Odelius, M. Hakkarainen, Carbonized lignosulfonate-based porous nanocomposites for adsorption of environmental contaminants, Functional Composite Materials. 1 (2020) 1–12. https://doi.org/10.1186/s42252-020-00008-8.

[73] S. Ersali, V. Hadadi, O. Moradi, A. Fakhri, Pseudo-second-order kinetic equations for modeling adsorption systems for removal of ammonium ions using multi-walled carbon nanotube, Fullerenes, Nanotubes and Carbon Nanostructures. (2013) 150527104639002. https://doi.org/10.1080/1536383x.2013.787610.